

# DETECTION AND CORRECTION OF SPECTRAL AND SPATIAL MISREGISTRATIONS FOR HYPERSPECTRAL DATA

Naoto Yokoya,<sup>1</sup> Norihide Miyamura,<sup>2</sup> and Akira Iwasaki<sup>2</sup>

<sup>1</sup>Department of Aeronautics and Astronautics, University of Tokyo, Japan

<sup>2</sup>Research Center for Advanced Science and Technology, University of Tokyo, Japan

\*E-mail: yokoya@sal.rcast.u-tokyo.ac.jp

## ABSTRACT

Hyperspectral imaging sensors suffer from spectral and spatial misregistrations. These artifacts prevent the accurate acquisition of the spectra and thus reduce classification accuracy. The main objective of this work is to detect and correct spectral and spatial misregistrations of hyperspectral images. The Hyperion visible near-infrared (VNIR) subsystem is used as an example. An image registration method using normalized cross-correlation for characteristic lines in spectrum image demonstrates its effectiveness for detection of the spectral and spatial misregistrations. Cubic spline interpolation using estimated properties makes it possible to modify the spectral signatures. The accuracy of the proposed postlaunch estimation of the Hyperion properties has been proven to be comparable to that of the prelaunch measurements, which enables the precise onboard calibration of hyperspectral sensors.

**Index Terms**— hyperspectral sensor, Hyperion, spectral misregistration, spatial misregistration

## 1. INTRODUCTION

Hyperspectral imaging sensors enable high-spectral resolution remote sensing, such as the precise classification of vegetation and mineral mapping. They collect spectrogram as a set of data cube, each of which represents a spectral band radiance. These images form a three-dimensional (3D) cube, composed of crosstrack ( $x$ ), line ( $y$ ) and spectrum ( $\lambda$ ) dimensions. Hyperspectral data contains hundreds to thousands of spectral bands. Owing to the high-resolution spectral profile in each pixel, it is possible to discriminate among land-cover classes that are spectrally similar [1].

Hyperspectral imaging sensors usually suffer from spectral and spatial misregistrations. Optical-system aberrations and misalignments cause these artifacts mainly due to push-broom systems, where crosstrack and spectral pixels are continuously recorded at the same time using a two-dimensional (2D) detector array. Spectral misregistration, also known as a “smile” curve, is a shift in wavelength in the spectral domain, which is a function of the crosstrack pixel number. Spatial misregistration, also called “keystone”, corresponds to

band-to-band misregistration. Both types of misregistration distort the spectral features and thus reduce classification accuracy.

The Hyperion is a hyperspectral imager onboard the Earth Observing 1 (EO-1) satellite launched on November 21, 2000. The Hyperion system, consists of visible near-infrared (VNIR) and short-wave infrared (SWIR) subsystems, and acquires data in 198 spectral bands. The Hyperion VNIR spectrometer obtains optical images of 50 bands over a range of 426.8-925.4 nm. In this work, the Hyperion VNIR is used as an example because the specification of the sensor is described well.

The main objective of this work is to detect and correct the spectral and spatial misregistration of hyperspectral image. An image registration using normalized cross-correlation for characteristic lines in the spectrum image, or the  $x$ - $\lambda$  plane, is used for detection and cubic spline interpolation is employed for correction of artifacts. First, detection methods and correction results for spectral and spatial misregistration are demonstrated, respectively. The change of the alignment of the sensor components at the launch is then investigated by a simulation of basic spectrometer model.

## 2. SPECTRAL MISREGISTRATION

Spectral smile becomes observable when the image is transformed into maximum noise fraction (MNF) space [2]. MNF transformation produces new components ordered by image quality by projecting the original image into a space where the new components are sorted in order of SNR. The most important procedure in MNF is to estimate the noise covariance matrix effectively. To get the noise covariance matrix, we estimate the signal part of each pixel. There are many various models that estimate the value  $\hat{s}_{x,y,\lambda}$ , the signal part of original value  $s_{x,y,\lambda}$ . To visualize the spectral smile clearly in low-order MNF, we adopt

$$\hat{s}_{x,y,\lambda} = \begin{cases} as_{x+1,y,\lambda} & (x < W) \\ as_{x-1,y,\lambda} & (x = W) \end{cases} (1 \leq y \leq H, 1 \leq \lambda \leq N), \quad (1)$$

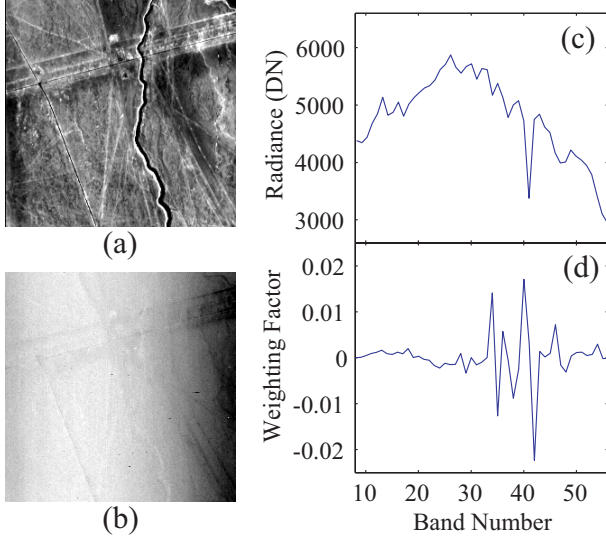


**Fig. 1.** (a)Original band 31, (b) MNF band 1 obtained from bands 8 to 57 of a desert scene in Chile, (c) spectral profile of the scene, and (d) weighting factors indicating the contribution to MNF1.

where  $W$  and  $H$  are the width and height of the image, respectively, and  $N$  is the total number of bands. The residual  $r = s - \hat{s}$  is the noise value of each pixel. The coefficient  $a$  is computed so as to minimize  $\sum r^2$ .

For Hyperion images with significant smile, there is a brightness gradient appearing in the first eigenvalue image, MNF1. Fig. 1 shows the MNF1 of bands 8 (426.8nm) to 57 (925.4nm) for a desert scene in Chile, the spectral profile of the scene, and the weighting factors that indicate the contribution to MNF1. In this case, MNF1 is mainly dominated by bands 40 (752.4nm) and 42 (772.8nm), near the oxygen absorption band 41 (762.6nm). This means that bands 40 and 42 are strongly affected by the smile effect because of distorted oxygen absorption line. Thus, we used the radiance difference between bands 40 and 42 as a spectral misregistration indicator.

The prelaunch spectral property of the Hyperion VNIR was characterized by the developer TRW using multispectral test bed [3]. Most researchers use TRW information to correct spectral misregistration. However, past research has shown that the prelaunch spectral property is changed after the launch [4, 5].

We estimated the spectral property of band 41 of the oxygen absorption line in the  $x$ - $\lambda$  plane using image registration by normalized cross-correlation. The normalized cross-correlation function between the source and destination sub-scenes in the line, which is calculated by Eq. (2), is shown at the bottom of the page.  $S(i, j)$  and  $D(i, j)$  denote pixel

$$C(m, n) = \frac{\sum_j^{L_\lambda} \sum_i^{L_x} \{S(i, j) - \bar{S}\} \times \{D(i - m, j - n) - \bar{D}\}}{[\sum_j^{L_\lambda} \sum_i^{L_x} \{S(i, j) - \bar{S}\}^2 \times \sum_j^{L_\lambda} \sum_i^{L_x} \{D(i - m, j - n) - \bar{D}\}^2]^{1/2}} \quad (2)$$

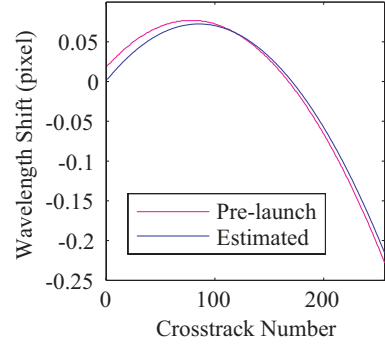


**Fig. 2.** Prelaunch and estimated spectral property of band 41.

values of the source and destination sub-scenes of  $(i, j)$ . The size of the correlation window  $(L_x, L_\lambda)$  is set as  $(1, 7)$  for detection of spectral misregistration. Using parabola fitting over three pixel grid points with their similarity, sub-pixel estimation of spectral misregistration  $\hat{D}_{spectral}$  is given by

$$\hat{D}_{spectral} = \frac{C(0, -1) - C(0, 1)}{2C(0, -1) - 4C(0, 0) + 2C(0, 1)}. \quad (3)$$

Along crosstrack direction this estimation can detect the distortion of the line, which shows smaller values because of “pixel-locking” effect [6]. Pixel-locking effect is the phenomenon that the estimated positions tend to be biased toward integer values depending on image characteristics, the similarity function, and the fitting function. By making a simulation data with applied smile property, we examined pixel-locking effect. After correction of pixel-locking effect, the spectral property of band 41 is finally determined. Estimated property is slightly different from the prelaunch property as shown in Fig. 2.

We have corrected bands 40 and 42 using cubic spline interpolation with the estimated spectral property and have evaluated the validity of the correction with the radiance difference between bands 40 and 42 those are much influenced by smile effect. Fig. 3 showed the radiance differences between bands 40 and 42. In the original data, the smile brightness gradient can be seen clearly. In the data corrected using prelaunch spectral property, there is a little brightness gradient because of overcorrection. In the data corrected using estimated spectral property, there is no brightness gradient. As a result, the estimated spectral property is proved to be valid based on MNF analysis and band-difference.

Spectral smile correction of band 41 has failed because cubic spline interpolation can not restore the original deep absorption spectrum. Thus, absorption bands should be avoided as a preparation in hyperspectral image processing, such as classification and band rationing.

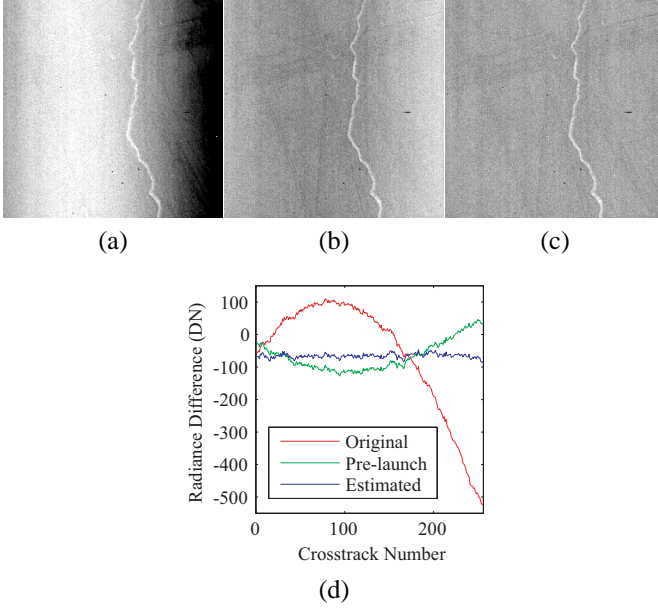


**Fig. 3.** The radiance differences between bands 40 and 42: (a) original spectral misregistration, (b) corrected by prelaunch spectral property, (c) corrected by estimated spectral property, and illustration of (d) horizontal profiles of (a)-(c).

### 3. SPATIAL MISREGISTRATION

The prelaunch spatial misregistration was measured at 20 locations using a point source [3]. The postlaunch spatial misregistration was also measured by TRW using lunar images obtained on orbit. However, this information is not attached to the Hyperion data. Therefore almost all users use the data without correcting spatial misregistration. Past studies on spatial misregistration detection proposed a scene-based method using edge detection by sharpening filter [7][8]. In this paper, a scene-based point source detection method is proposed for detection of the postlaunch spatial misregistration.

First, point source subscenes where the radiance is high in many spectral channels on the homogeneous background are detected. We estimate the spatial misregistration using image matching for this spectral direction along the bright spectral line in the  $x$ - $\lambda$  plane as the same way as in the detection of the spectral smile. The size of the correlation window  $(L_x, L_\lambda)$  is set as  $(7, 1)$  for detection of spatial misregistration. Band 31 (660.9nm) was chosen as the reference because of its central position in Hyperion VNIR spectral dimension in the  $x$ - $\lambda$  plane and relatively high SNR. Sub-pixel estimation of spatial misregistration  $\hat{D}_{spatial}$  is given by

$$\hat{D}_{spatial} = \frac{C(-1, 0) - C(1, 0)}{2C(-1, 0) - 4C(0, 0) + 2C(1, 0)}. \quad (4)$$

This approach was carried out on the Cuprite site acquired

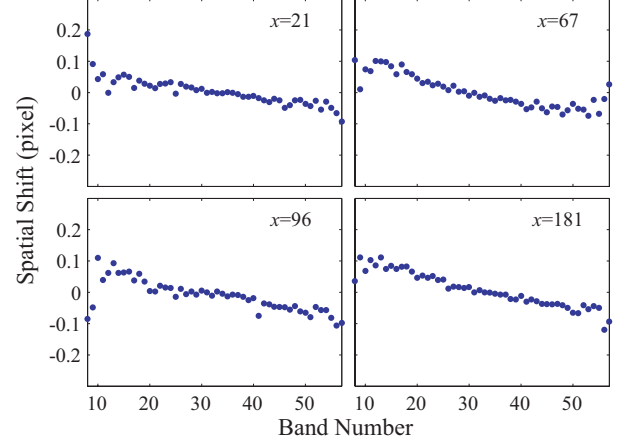


**Fig. 4.** Spatial misregistration for four crosstrack positions.

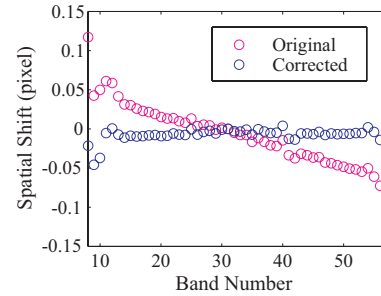


**Fig. 5.** Comparison of spatial misregistration estimated using full scenes.

on March 4, 2002. Similar keystone patterns were obtained in various crosstrack numbers, as shown in Fig. 4. We assumed that the spatial misregistration was constant in all crosstrack numbers. Fig. 5 shows the spatial misregistration of the Hyperion VNIR has been successfully corrected using cubic spline interpolation. Fig. 6 presents MNF transformation results for a desert scene in Chile. After correction of both spectral and spatial misregistrations, dry rivers that can be clearly seen in MNF2 has appeared in MNF1 (compare the portions indicated by arrows in (a) and (b) in Fig. 6). It indicates that the proposed detection and correction method improves Hyperion VNIR image quality.

### 4. SPECTROMETER MODEL

The change in the alignment of the Hyperion VNIR components at the launch has been considered qualitatively by a simulation of basic spectrometer model. The main specification of this simulation is as follows: view angle is 3 degrees, grating frequency is 1000 lines/mm, and focal point distance is 100 mm. Spot diagram is obtained by rotating mounting angles of slit, grating, and 2D detector array. Fig. 7 shows the spot diagrams in the cases where mounting angles of slit,

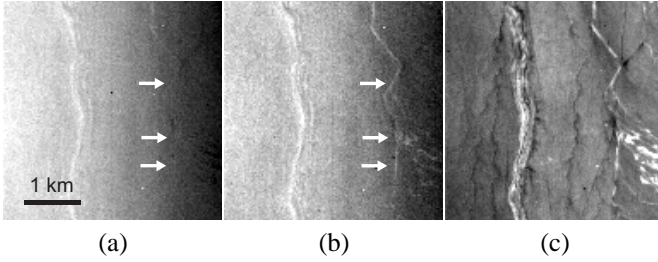


**Fig. 6.** MNF1s of (a) before and (b) after correction of spectral and spatial misregistration, and (c) MNF2 after correction.

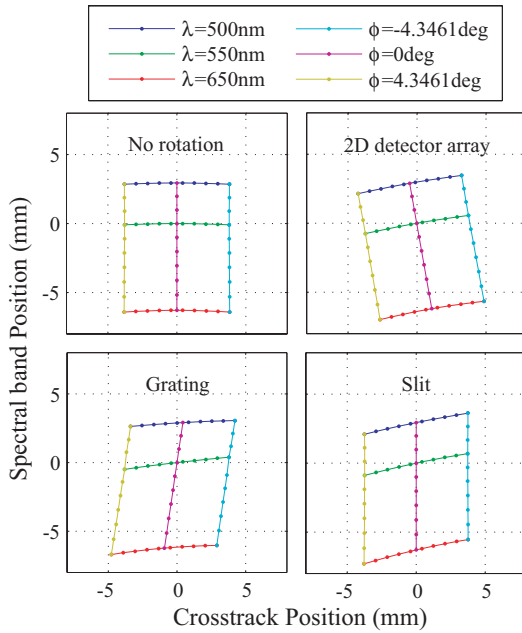


**Fig. 7.** Basic spectrometer simulations in which mounting angles of slit, grating, and 2D array are rotated in 10 degrees around light axis.

grating, and 2D array are rotated in 10 degrees around light axis.

This simulation and the comparison with the Hyperion spectral and spatial properties between prelaunch and post-launch can suggest the possible cause of the misalignment at the launch. It was impossible to obtain the accurate change of spatial property because the prelaunch spatial property was not public. As demonstrated in previous section, the spatial misregistration of Hyperion VNIR was approximated at a linear function of band number. In the case that the absolute gradient of this linear function has changed smaller, 2D array may have rotated. In contrast, if it has changed larger, slit of grating may have rotated. Thus, numerically accurate prelaunch spatial property makes it possible to estimate the origin of the change of sensor characteristics at the launch.

## 5. CONCLUSIONS

This paper has proposed a postlaunch estimation method for hyperspectral sensor characteristics. The image registration by normalized cross-correlation for characteristic lines in the spectrum image can detect spectral and spatial misregistration for the Hyperion VNIR. Using oxygen absorption line, spectral misregistration of band 41 is obtained. A scene-based point source subscene where the radiance is high in many spectral channels enables the detection of the spatial misregistration for each crosstrack number. Cubic spline interpolation using estimated properties has shown its effectiveness for correction of the spectral and spatial misregistration and the validity of the estimated Hyperion VNIR characteristics. The accuracy of proposed postlaunch estimation of the Hyperion properties is comparable to that of the prelaunch measurements, which enables the precise onboard calibration of hyperspectral sensors.

## 6. REFERENCES

- [1] F. A. Kruse, J. W. Boardman, and J. F. Huntington, "Comparison of airborne hyperspectral data and EO-1 Hyperion for mineral mapping," *IEEE Trans. Geosci. Remote Sens.*, vol. 41, no. 6, pp. 1388-1400, 2003.
- [2] A. A. Green, M. Berman, P. Switzer, and M. D. Craig, "A transformation for ordering multispectral data in terms of image quality with implications for noise removal," *IEEE Trans. Geosci. Remote Sens.*, vol. 26, no. 1, pp. 65-74, Jan. 1988.
- [3] TRW Space, Defense and Information Systems, "EO-1/Hyperion Early Orbit Checkout Report Part2 : On-orbit Performance Verification and Calibration," pp. 107-111, 2002.
- [4] J. S. Pearlman, P. S. Barry, C. C. Segal, J. Shepanski, D. Beiso, and S. L. Carman, "Hyperion, a space-based imaging spectrometer," *IEEE Trans. Geosci. Remote Sens.*, vol. 41, no. 6, pp. 1160-1173, 2003.
- [5] R. A. Neville, L. Sun, and K. Staenz, "Detection of spectral line curvature in imaging spectrometer data," *Proc. of the SPIE*, vol. 5093, pp. 144-154, 2003.
- [6] J. Westerweel, "Effect on sensor geometry on the performance of PIV interrogation," *Proc. 9th International Symposium on Applications of Laser Techniques to Fluid Mechanics*, page 1.2, 1998.
- [7] R. A. Neville, L. Sun, and K. Staenz, "Detection of keystone in imaging spectrometer data," *Proc. of the SPIE*, vol. 5425, pp. 208-217, 2004.
- [8] F. Dell'Endice, J. Nieke, D. Schlapfer, and K. I. Itten, "Scene-based method for spatial misregistration detection in hyperspectral imagery," *Applied Optics*, vol. 46, no. 15, pp. 2803-2816, 2007.